ACS APPLIED NANO MATERIALS

www.acsanm.org Article

Homogeneous Nanostructuring of a Molybdenum Surface by Dual-Color Correlated Femtosecond Laser Irradiation for Solar Absorber Applications

Bo Zhao,[#] Ruiping Wang,[#] and Jianjun Yang*

Cite This: *ACS Appl. Nano Mater.* 2023, 6, 21092−21100 Read Online

ACCESS | Metrics & More | Article Recommendations

ABSTRACT: Disordered ridge-splitting on laser-induced periodic surface structures (LIPSSs) often reduces structure quality and degrades application performance but introduces a potential route for laser structuring accuracy with access to the deep-subwavelength scale. Here, nanolithography based on the homogeneous ridge-splitting mechanism is implemented on a molybdenum surface using two-color (400 and 800 nm) temporally delayed femtosecond laser pulses with identical linear polarizations. The achieved splitting LIPSS, with a periodicity down to 140 nm and a feature size down to 70 nm, was uniformly distributed in the long range without any wavy or interruption defects, presenting improvements on the structure's accuracy and quality relative to the observation of single-beam femtosecond 400 nm laser irradiation. The generation and suppression of the homogeneous ridge-splitting phenomenon can be manipulated via altering the time delay or the fluences of the two-color laser pulses, which results in transitions between the regular near-subwavelength and deep-subwavelength LIPSSs. The underlying physical origins are attributed to the excitation of various electromagnetic field enhancement modes during the transiently correlated dynamic process of two-color laser−material interactions. Our investigations facilitate the laser nanostructuring of metals with an accessible 100 nm feature size, and the nanostructured Mo surface enables specific applications in the field of concentrated solar energy devices.

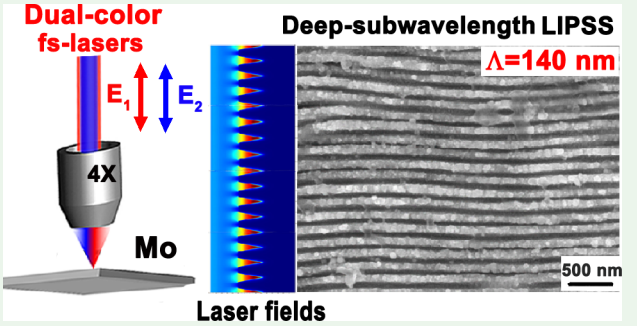

KEYWORDS: *laser-induced periodic surface structure, deep-subwavelength, homogeneous ridge-splitting, two-color femtosecond lasers, solar absorber, molybdenum, local electromagnetic mode, transient dynamic*

1. INTRODUCTION

The phenomenon of the laser-induced periodic surface structures (LIPSSs) is commonly observed upon irradiation of the linearly polarized femtosecond laser pulses on a variety of materials, especially with the fluence nearly below the ablation threshold.[1−8] The LIPSS usually exhibits a periodic distribution of ablation lines, in which the spatial orientation strictly depends on the laser polarization, while the period is closely related to the laser wavelength and material properties. Currently, the underlying mechanisms of LIPSSs are still in debate, which include the theory of interference between the excited surface electromagnetic (EM) waves with the incident laser and the self-organization from Marangoni convective instabilities.[1,2] The interference theory is widely accepted for the origin of low-spatial-frequency LIPSSs, while the self-organization theory is generally ascribed to the formation mechanism of the high-spatial-frequency LIPSSs. Importantly, the development of LIPSSs can refunctionalize material surfaces for new applications in optics, tribology, biology, wettability, etc.[9−14] Moreover, LIPSSs can be achieved with a one-step and mask-free procedure to provide an efficient and flexible surface micro/nanostructuring technology, which overcomes the disadvantages of low throughput and complexity observed in the conventional lithography.[15,16] In most cases, LIPSS formation is a result of multipulse irradiation, associated with positive feedback from the pulse-to-pulse surface morphology change. During the multipulse ablation feedback process, grating-assisted laser−SPP coupling is apt to induce the local EM field enhancement on the ridge surfaces, leading to the splitting phenomenon.[17−19]

Usually, the ridge-splitting observation features disorder and chaos, especially under the single-beam femtosecond laser irradiation, which disturbs the spatial alignment of the structures and induces an irregular and semiperiodic

Received: August 30, 2023
Revised: October 18, 2023
Accepted: October 19, 2023
Published: November 4, 2023

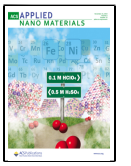

appearance accompanied by bending, forking, and interruption defects.[17−19] Such poor quality of the surface structures definitely degrades the applicable performance of the relevant devices. On the other hand, however, this process introduces a potential halving of the structure period toward the deep-wavelength scales with high spatial regularity. Although the "static" control of the ridge-splitting phenomenon was explored by changing both the laser fluence and the pulse number accumulation of single-beam femtosecond laser irradiation, there is no substantial improvement in the structure quality.[17−19] Noticeably, recent research has demonstrated that temporally shaped femtosecond laser pulse irradiation can provide an approach for the manipulation of LIPSSs via correlating the transient dynamic of the laser−material interactions.[20−27] For example, with irradiation of two/three/multiple time-delayed femtosecond laser pulses, the morphologic characteristics of the LIPSS, including the geometric shape, period, orientation, and regularity, can be selectively manipulated by varying the time delay, the laser wavelength, the fluence ratio, and the polarization state. Nevertheless, the actively "dynamic" control of the ridge-splitting phenomenon using the temporally shaped femtosecond laser pulse irradiation has been less explored.

In this paper, two-color temporally delayed femtosecond laser pulses with identical linear polarizations are utilized to actively and dynamically control the ridge-splitting phenomenon on a molybdenum (Mo) surface. Based on the generation and suppression of the homogeneous ridge-splitting phenomenon, we achieved highly regular near-subwavelength LIPSSs (NSL) and deep-subwavelength LIPSSs (DSL) as well as the transitions between them. The physical origins are elaborated on by numerically simulating the excitation of different types of EM enhancement modes under the dual-color correlated femtosecond laser pulse irradiation. The dual-color correlated laser nanostructuring not only provides a strategy for manufacturing structures on metals with 100 nm feature sizes but also renders new functions by altering its properties in optics, mechanics, chemistry, and biology. The nanostructured Mo surface not only displays performance improvements on solar absorptance and selectivity, which are beneficial for efficient solar absorber applications,[5,28] but also enables other potential applications in antifriction, antibacteria, biocompatibility, superhydrophobicity, etc.

2. MATERIALS AND METHODS

Figure 1 illustrates a diagram of an interferometer-like experimental setup for producing the uniform 100 nm LIPSSs on the Mo surface upon irradiation of two-color temporally delayed femtosecond lasers with identical linear polarizations. First, the infrared wavelength (800 nm, 1 kHz, 50 fs) of the linearly polarized laser pulse trains that are delivered from a commercial Ti:sapphire laser amplifier system (Spectra Physics HP-Spitfire 50) are incident to the Michelson interferometer-like optical design. After passing through a beam splitter, each laser pulse was spatially separated into two subpulse beams along different optical paths, and their delay in the time domain can be precisely adjusted within a range of $-300\ \text{ps} < \Delta t < +300\ \text{ps}$ via a delay-line configuration. Within one of the optical paths, a β-barium-borate (BBO) crystal was inserted to generate the 400 nm laser via frequency doubling, which was followed by a spectral band-pass filter to eliminate the fundamental 800 nm laser components. The polarization direction of the 800 nm laser in the other optical path was tuned parallel to that of the 400 nm laser through a half-wave plate. Afterward, the two-color laser beams were spatially aligned into an overlapping collinear propagation via another beam splitter and then focused by an achromatic objective lens (RMS4X, Olympus) onto the sample surface at normal incidence. The positive time delay indicates the arrival of the 800 nm laser pulse prior to the 400 nm one. The energies of the two-color lasers can be adjusted separately via the neutral density filters.

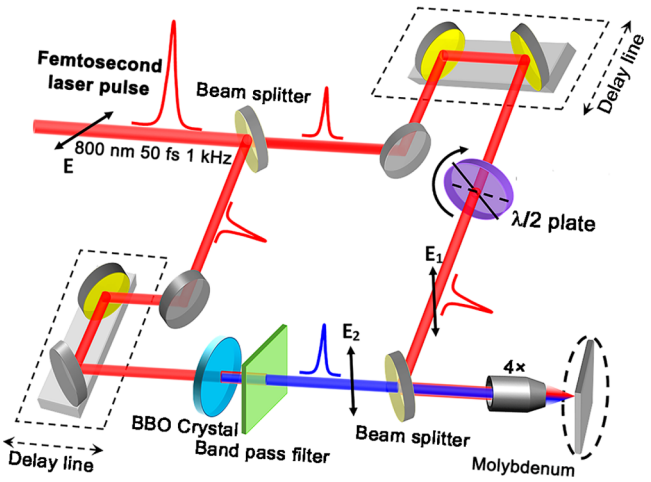

Figure 1. Schematic of the experimental setup for the homogeneous nanostructuring of metal surfaces using two-color temporally delayed femtosecond lasers that are generated by a Michelson interferometer-like optical design. The parallel linear polarizations of the 800 and 400 nm lasers are represented by E_1 and E_2, respectively.

A mechanically polished Mo plate with a purity of 99.98% was selected as the sample because of its high elasticity modulus and its thermal and electrical conductivity properties, which are useful for wide applications in microelectronics, photoelectronics, laser and space optics, and fusion reactors.[29,30] The experiments were implemented with a line-scanning method through the precise translation of the sample via a computer-controlled X-Y-Z stage (Newport, UTM100 PPE1). The focal laser spot on the sample surface, which was placed at a position 400 mm away from the focus to avoid air ionization disturbance, was measured as $2\omega_0 = 80\ \mu\text{m}$ ($1/e^2$ peak intensity) in diameter. The adopted translating speed of $v = 0.1$ mm/s results in 800 laser pulses partially overlapping within the laser spot area. The fluence of the laser pulse was estimated by $F = 2E_0/\pi\omega_0^2$,[1] with E_0 being the pulse energy. Before and after the experiments, the sample surfaces were ultrasonically cleaned in an acetone solution. The laser-induced surface morphologies were characterized by scanning electron microscopy (SEM; Hitachi, S-4800).

3. EXPERIMENTAL RESULTS AND DISCUSSION

First, we investigated the LIPSS behavior on the Mo material with a single beam of the 400 nm femtosecond laser irradiation. The surface morphology at a fluence of $F = 0.088\ \text{J/cm}^2$ is shown in Figure 2a. Clearly, the so-called LIPSS with the spatial orientation perpendicular to the laser polarization is actually constituted by the irregular distribution of ablation grooves having wavy and interruption defects, which is similar to the observations in many previous reports.[17−19] Moreover, splitting traces can be found on the groove ridges in some localized regions. The measured average spatial period approximates $\Lambda = 280$ nm, belonging to the NSL regime. The measurement of the groove width is as narrow as $w = 80$ nm. With either increasing the laser fluence or decreasing the translation speed, the splitting traces become more pronounced and halve the structure period to 140 nm, as shown in Figure 2b, which enters the DSL regime. The corresponding spatial frequency image of the structure based on calculations of the two-dimensional fast Fourier transformation (2D-FFT) method is illustrated in Figure 2c, where a dense scattering distribution of data points indicates the worse situation in the spatial alignment. On the other hand, according to ref 31, the dispersion in the structure orientation angle (DSOA) for the NSL structure was

https://doi.org/10.1021/acsanm.3c03994
ACS Appl. Nano Mater. 2023, 6, 21092−21100

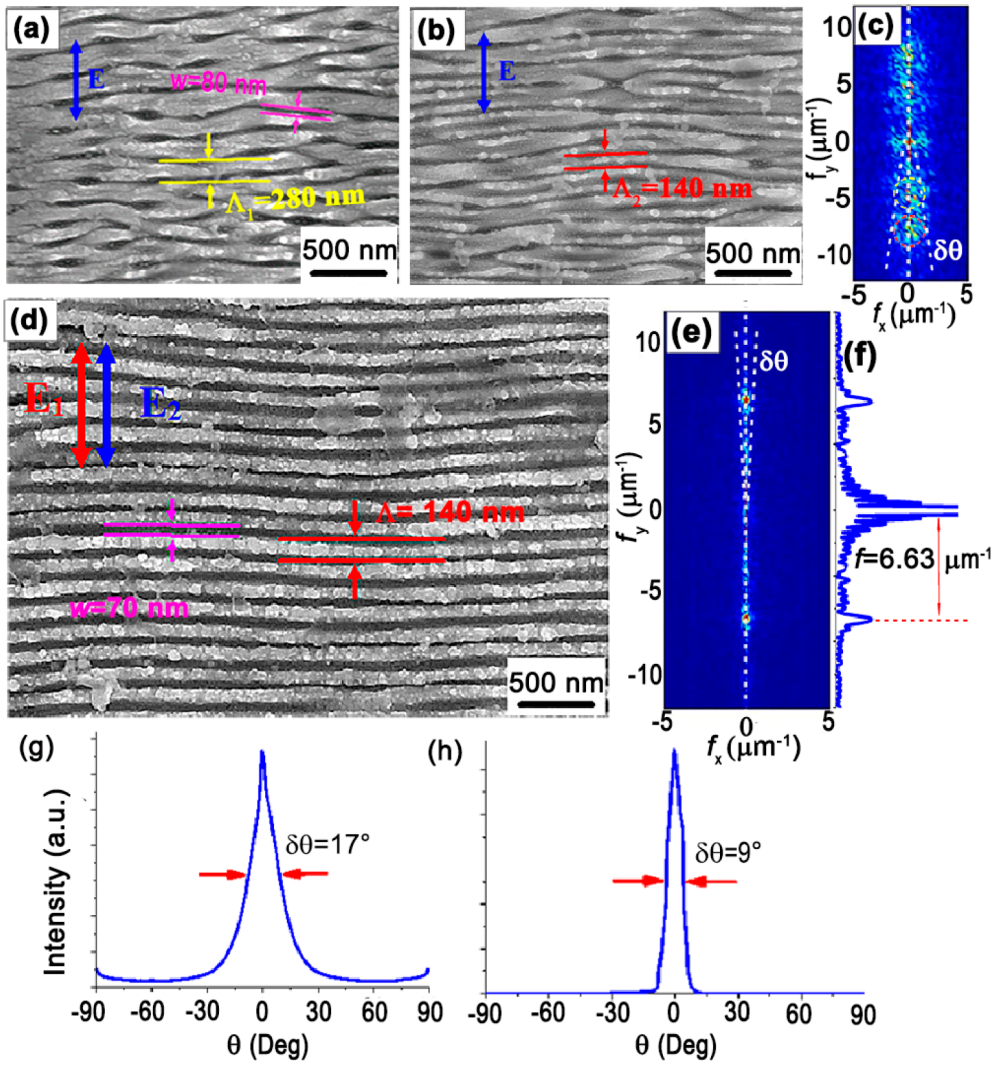

Figure 2. Characterization of the LIPSS on the Mo surface. (a and b) SEM images of the NSL formed under the irradiation of a single-beam 400 nm femtosecond laser with a fluence of F = 0.088 and 0.123 J/cm^2, respectively. (c) 2D-FFT image of the structure in (b). (d) SEM image of the uniform DSL formed under the irradiation of two-color temporally delayed femtosecond lasers with fluences of F_{400} = 0.088 J/cm^2 and F_{800} = 0.068 J/cm^2. (e) 2D-FFT image of the structure in (d). The red and blue double arrows represent the linear polarization directions of the 800 and 400 nm laser pulses, respectively. The time delay between the two-color laser pulses is 100 ps. (g and h) Calculated curve of the structure orientation angle distribution for the structures in (b) and (d), respectively.

calculated to quantitatively characterize the spatial alignment regularity. The obtained result of $\delta\theta$ = 17° in Figure 2g indicates the poor structure quality induced by the single-beam 400 nm femtosecond laser.

On the other hand, when irradiation of the two-color femtosecond laser pulses was introduced with a time delay of 100 ps and identical linear polarizations, the ridge-splitting phenomenon on the Mo surface could be manipulated into homogeneous behavior via the correlated dynamic between the dual laser−material interaction processes. Here, the 800 nm laser pulse is incident ahead of the 400 nm laser pulse, and the available fluences for the two-color laser pulses were set as F_{800} = 0.068 J/cm^2 and F_{400} = 0.088 J/cm^2, respectively, wherein the 800 nm one is less than the ablation threshold of the material. As shown in Figure 2d, the obtained grooves seem to possess a spatially continuous and periodic arrangement in the long range without any wavy or interruption problems. The measurement of the spatial period for such laser-induced grating is decreased down to Λ = 140 nm, belonging to the DSL regime. The measured groove width of about w = 70 nm as well as the ridge width of 70 nm display the structuring accuracy on the 100 nm scale. The straight arrangement of the parallel grooves associated with the sharp-edged profiles indicate the improvement on the structure quality, which is in contrast to the results of the single-beam 400 nm femtosecond laser irradiation. Accordingly, the calculated spatial frequency image of the aforementioned DSL is shown in Figure 2e, where the discrete distribution of the local points indicates high structural regularity in the spatial domain. The retrieved data for the frequency points are shown in Figure 2f, in which the measured frequency interval of f = 6.63 μm^{-1} corresponds to the reciprocal spatial period of 150 nm. Moreover, the calculated DSOA value of the DSL structures, as shown in Figure 2h, drops down to $\delta\theta$ = 9°, indicating the improvement in the regularity of the structures compared with the results of the single-beam 400 nm femtosecond laser. These results imply that the temporally delayed two-color femtosecond laser irradiation can be a powerful approach to generate the ridge-splitting phenomenon with large-area homogeneity.

To evaluate the physical action of the first incidence of the 800 nm femtosecond laser on the ridge-splitting generation, we investigated the evolution of the structure morphology with the time delay between the two-color laser pulses. The typical results are displayed in Figures 3a−d, where the fluences of the two-color laser pulses are maintained the same as those in Figure 2d. Clearly, at the time delay

https://doi.org/10.1021/acsanm.3c03994
ACS Appl. Nano Mater. 2023, 6, 21092−21100

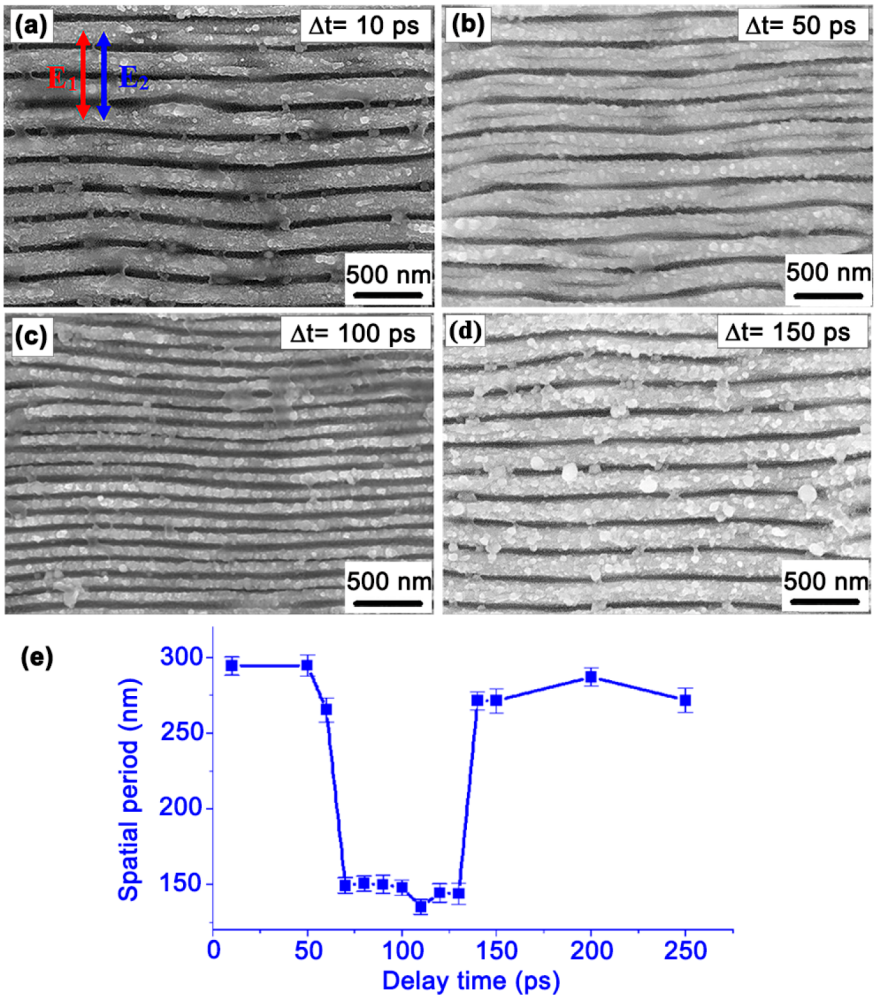

Figure 3. Evolution of the structure morphology with the time delay between the two-color laser pulses. (a–d) SEM images of the LIPSS at the variable time delay of Δt = 10, 50, 100, and 150 ps, respectively. (e) Measured spatial period as a function of the time delay in the range of Δt = 10–250 ps. The fluences of the two-color laser pulses are fixed as the same as those in Figure 2d.

of Δt = 10 ps, the laser-induced surface structure tends to have regular profiles and the NSL feature by possessing a spatial period of Λ = 280 nm, and its straight and continuous alignment is in sharp contrast to the observations of the single-beam 400 nm laser irradiation. With increasing the time delay to Δt = 50 ps, the NSL feature of the surface structure can be still formed, but it is accompanied by shallow fragmentary traces on the ridge areas. As the time delay approaches Δt = 100 ps, the splitting traces uniformly develop into new grooves with depths and widths identical to those of the original NSL, leading to complete transformation into the DSL. When the time delay continuously enlarges to Δt = 150 ps, the laser-induced structure returns to the NSL profiles without the splitting traces, very similar to the result at the time delay of Δt = 10 ps. The measured LIPSS period as a function of the time delay within a range of Δt = 10–250 ps is summarized in Figure 3e. It was found that the grating–splitting phenomenon is inclined to take place in the moderate time delay range of Δt = 60–130 ps, while it can be suppressed within either the short time delay range of Δt = 10–50 ps or the long time delay range of Δt = 140–250 ps. Moreover, in comparison to the case of the single laser beam irradiation, the two types of LIPSSs with the two time-delayed laser pulses are always observed to regularly align within the long range, indicating the contribution of the pre-irradiation of the 800 nm femtosecond laser pulse.

To gain deep insights into the interplay between dual-color laser–material interactions, we also investigated the influence of the two laser fluences on the ridge-splitting phenomenon. The experimentally obtained evolution of the LIPSS with 800 nm laser fluence is shown in Figures 4a–d, where the 400 nm laser fluence and the time delay between the two-color lasers are fixed as F_{400} = 0.088 J/cm^2 and Δt = 100 ps, respectively. It is obvious that the increase of the pre-irradiated 800 nm laser fluence can give rise to different degrees of ridge-splitting. As shown in Figure 4a, for the small 800 nm laser fluence of F = 0.054 J/cm^2, the ordinary NSL is formed with a shallow splitting depth on most of ridges. With increasing the 800 nm laser fluence to F = 0.068 J/cm^2, the ridge-splitting is more pronounced and becomes almost identical to the bilateral grooves, which indicates the complete transition from the usual NSL into the regular DSL. When the 800 nm laser fluence increases to F = 0.09 J/cm^2, which exceeds that of the 400 nm laser pulse, the ridge-splitting again appears to be shallow in depth compared to the grooves, indicating the onset of the DSL-to-NSL transition. In particular, as the 800 nm laser fluence further reaches the high value of F = 0.128 J/cm^2, the ridge-splitting traces seem to disappear entirely, leaving the regular distribution of NSL profiles on all of the laser-exposed areas.

The measured dependence of the LIPSS period on the pre-irradiated 800 nm laser fluence is shown in Figure 4e. It is seen that the structure period begins to jump from Λ = 140 to Λ = 280 nm at the 800 nm laser exceeding the fluence of F = 0.09 J/cm^2. On the other hand, how the LIPSSs develop while varying the fluence of the delayed 400 nm laser was studied as well, and the results are shown in the SEM images in Figures 4a, c, f, and g. Clearly, when the 400 nm laser fluence increases, the ridge-splitting behavior tends to be more pronounced with deepening grooves. Simultaneously, more generation of nanoscale grains and clusters can be found on the LIPSS

https://doi.org/10.1021/acsanm.3c03994
ACS Appl. Nano Mater. 2023, 6, 21092–21100

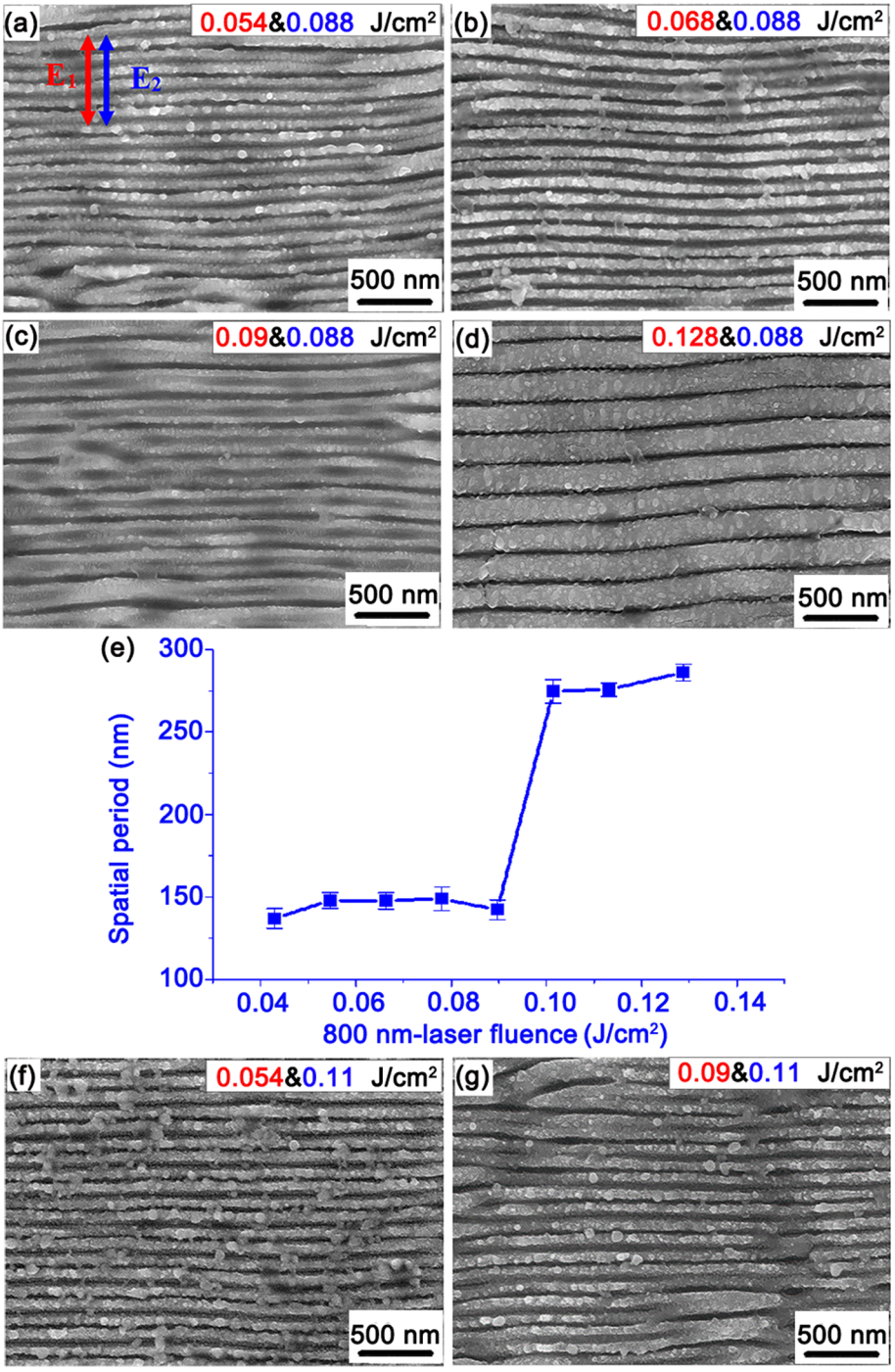

Figure 4. Influence of the two laser fluences on the ridge-splitting phenomenon. (a–d) SEM images of the LIPSS at different 800 nm laser fluences of F_{800} = 0.054, 0.068, 0.09, and 0.128 J/cm^2, respectively, associated with the fixed 400 nm laser fluence of F_{400}= 0.088 J/cm^2. (e) Measured spatial period as a function of the 800 nm laser fluence. (f and g) SEM images of the LIPSS at different 800 nm laser fluences of F_{800} = 0.054 and 0.09 J/cm^2, respectively, associated with the fixed 400 nm laser fluence of F_{400} = 0.11 J/cm^2. The time delay was set as Δt = 100 ps.

regions, which is due to the increased sputtering effect of thermal molten materials during the structure formation. In general, it can be reasonably deduced that the adopted fluences of dual-color femtosecond laser pulses affect the time delay points for both initiating and terminating the ridge-splitting phenomenon.

According to the commonly accepted electromagnetic theory of LIPSSs,[32−34] the excitation of surface plasmon polariton (SPP) and its subsequent interference with the incident laser field can modify the smooth energy distribution into spatially periodic patterns on the material's surface, which finally bring forth permanent grating-like ablation structures via the selective removal of materials. Usually, the observation of LIPSSs results from the multipulse accumulation process, wherein the laser-induced surface morphology changes from the random nanostructures to the nascent LIPSSs and then grows into the well-defined alignment via the positive feedback of the SPP−laser coupling.[17−19] At the early stage of the multipulse feedback process, the SPP−laser coupling mediated by the nanostructures is inclined to promote the growth of LIPSSs, and vice versa. Meanwhile, at the later stage of this process, upon irradiation of the already existing nascent LIPSSs by the subsequent laser pulses, the grating-assisted SPP−laser coupling is prone to trigger local EM field enhancement, especially on the center area of the ridges, which produces the ridge-splitting

https://doi.org/10.1021/acsanm.3c03994
ACS Appl. Nano Mater. 2023, 6, 21092−21100

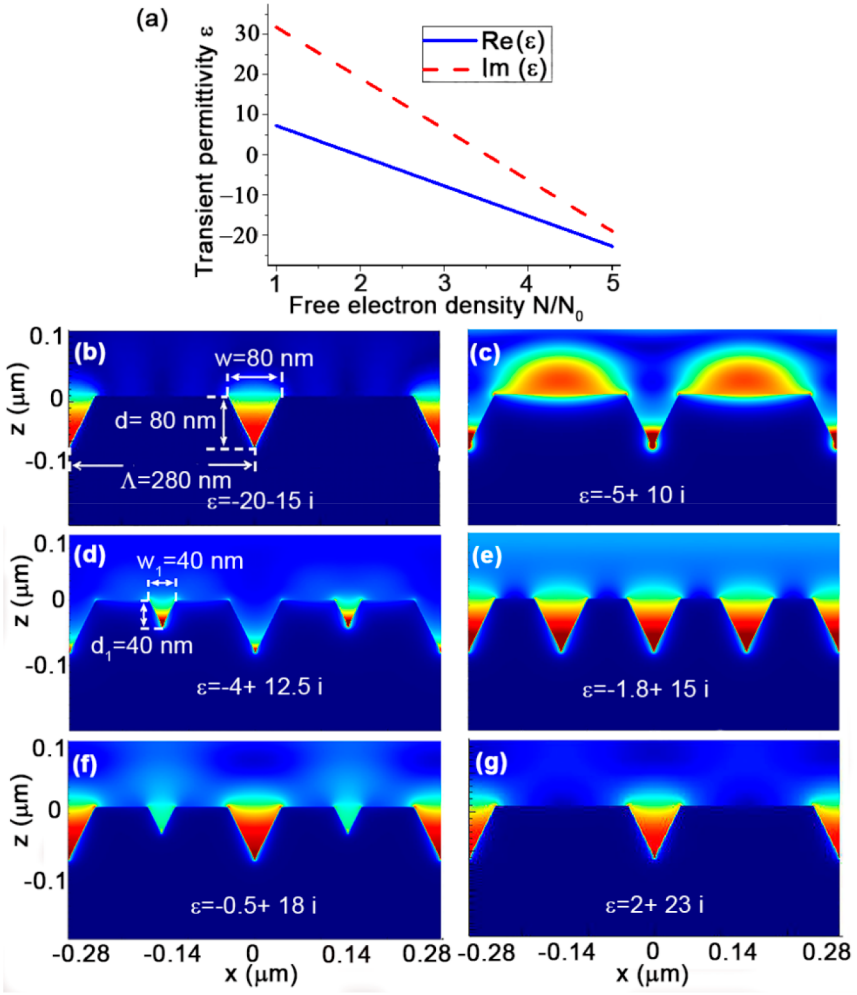

Figure 5. Simulated spatial distributions of the electromagnetic field on the V-shaped groove with different optical permittivity ε values under the normal incidence of a TM-polarized light with a laser wavelength of λ = 400 nm. (a) Dependence of the transient permittivity on the excited free electron density. (b) $\varepsilon = -20-15i$. (c) $\varepsilon = -5 + 10i$. (d) $\varepsilon = -4 + 12.5i$. (e) $\varepsilon = -1.8 + 15i$. (f) $\varepsilon = -0.5 + 18i$. (g) $\varepsilon = 2 + 23i$.

phenomenon. However, under the irradiation of single-beam femtosecond laser pulses, the spatially nonuniform distribution of the splitting traces brings about poor structure quality, as shown in Figures 2a and b. The previous simulation investigations demonstrated that the laser-induced local EM field enhancement for the ridge-splitting is closely dependent on the permittivity (ε) of the material's surface.[17−19] Under the single-beam femtosecond laser irradiation at a repetition rate of 1 kHz, the inherent long time interval of 1 ms between two neighboring pulses makes the transient permittivity of the material's surface inflexible during the multipulse feedback process, so that the aforementioned two ways for improving the poor quality of the splitting LIPSSs are invalid.[17−19] In our experiment, however, control of the ridge-splitting phenomenon implies that the material permittivity and its supporting EM field distribution can be manipulated via the transiently correlated dynamic of the two-color laser−material interactions.

In the case of Mo metal, the tabulated value of the permittivity is Mo = 7.26 + 31.8i for the laser wavelength of λ = 400 nm,[35] whose positive value in the real part indicates no support of the SPP excitation. Upon femtosecond laser irradiation, the transient change of the material permittivity on the surface is related to the pulse energy when considering the contribution from the interband absorption, which concerns a transition of electrons from the ground state to the excited state via single or multiphoton absorption to become free electrons.[36,37] This can help increase the plasma frequency, leading to decreased transient permittivity of ε. In other words, after the laser pulse energy deposition, the real part of the permittivity on the material's surface can be instantaneously reduced to negative values. Notably, such a permittivity reduction can only be maintained during the short time duration of the electron relaxation, after which the disappearing excited free electrons promote the real part of the permittivity toward positive values. Based on the Drude model, we have numerically estimated the dependence of the transient permittivity on the excited free electron density, as shown in Figure 5a.

In our dual-color femtosecond laser experiment, the birth of the nascent LIPSS on the Mo surface is dominated by the time-delayed irradiation of the 400 nm laser pulse because of the observed surface structures having a spatial period of 280 nm. Or we can understand that the LIPSS embryon of the 800 nm laser pulse is smeared out by the time-delayed 400 nm laser pulse incidence. For the succeeding irradiation of dual-color laser pulse pairs on the nascent LIPSS, the incident 800 nm laser pulse is dedicated to modifying the material permittivity via the interband absorption owing to the fluence below the ablation threshold of the material. As a result, the transient change of the permittivity is doomed to affect the 400 nm laser pulse field distribution on the nascent LIPSS, so that the ridge-splitting phenomenon can be manipulated. This hypothesis can be confirmed by the simulation results with the finite-difference time-domain (FDTD) method. Here, a periodic distribution of V-shaped grooves is employed for the nascent LIPSS, whose geometric parameters are given by a width of w = 80 nm, a period of Λ = 280 nm, and a depth of d = 80 nm, according to the experimental measurements. The

https://doi.org/10.1021/acsanm.3c03994
ACS Appl. Nano Mater. 2023, 6, 21092−21100

incident light source is a plane wave at a wavelength of 400 nm with TM polarization.

Figure 5 illustrates the evolution of the time-averaged Poynting vector for the EM field distribution on the periodic V-shaped groove structure with different transient permittivity values. As shown in Figure 5b, when the transient permittivity is assumed to be $\varepsilon = -20 - 15i$, the simulated EM field enhancement is localized within the subwavelength grooves with almost no intensity on the ridges. Such groove-preferring energy deposition benefits the suppression of the splitting phenomenon to generate the regular NSL, which corresponds to the observations of dual-color femtosecond laser irradiation with the short time delay range of $\Delta t = 10-50$ ps. On the other hand, as the transient permittivity increases to $\varepsilon = -5 + 10i$, it is revealed that the simulation of EM field enhancement begins to emerge on the ridge areas, as shown in Figure 5c. This kind of ridge-preferring energy deposition can ablate the material to initiate ridge-splitting on the NSL, and it tends to develop into new grooves with the succeeding irradiation of multiple laser pulses, which corresponds to the observation of dual-color femtosecond laser irradiation at a time delay of $\Delta t = 60$ ps.

The simulation of the EM field distribution on the NSL with some new small trenches on the ridge surface is shown in Figure 5d, where the transient permittivity of the material's surface is adopted as $\varepsilon = -4 + 12.5i$. In this case, the enhanced EM field intensity is concentrated within the new trenches, which contributes to their further expansion in both the width and the depth. As long as the trenches grow to be the same as the peripheral grooves, the EM field enhancement is observed to equally distribute within them, especially for the enlarged transient permittivity of $\varepsilon = -1.8 + 15i$, as shown in Figure 5e. Such groove-preferring energy deposition can account for the DSL formation under the dual-color femtosecond laser irradiation with the time delay of $\Delta t = 100$ ps. With increasing the transient permittivity to $\varepsilon = -0.5 + 15i$, the ridge-preferring EM field enhancement dominated by the excitation of the evanescent quasi-cylindrical surface wave (QSW), rather than SPP, becomes weakened while the groove-preferring enhancement gets strengthened,[38,39] as displayed in Figure 5f, which corresponds to the depression of the ridge-splitting behavior on the NSL. Of course, when the transient permittivity becomes $\varepsilon = 2 + 23i$, the ridge-preferring EM field enhancement based on the QSW excitation is found to fade away and transfer into the groove-preferring mode, as shown in Figure 5g, which corresponds to the generation of the regular NSL at the long time delay of $\Delta t = 150$ ps.

Overall, the LIPSS morphology obtained by dual-color femtosecond laser irradiation closely depends on the enhanced EM field distribution on the material's surface, which in fact varies with the time delay change of the transient permittivity. Through combining the experimental results and theoretical simulations, we have a comprehensive understanding of the physical pictures for the control of the ridge-splitting phenomenon with the time-delayed dual-color femtosecond laser pulse irradiation. The groove-preferring EM field enhancement, which is supported by the nascent LIPSS with a large negative value of the transient permittivity at the short time delay, gives birth to the regular NSL via the effective suppression of the ridge-splitting phenomenon. The increase of transient permittivity with the time delay helps transform the EM field enhancement into the evident ridge-preferring mode, which is the physical origin for the ridge-splitting phenomenon based on the feedback of multipulse pair irradiation.

When the transient permittivity of the material's surface increases to the proper values at modest time delays, the ridge-preferring EM field enhancement evolves into the groove-preferring mode, which is responsible for the generation of the regular DSL. With continuing the time delay elongation, the increase of the transient permittivity makes the EM field enhancement gradually reverse back to the groove-preferring mode, so that the regular formation of NSL is achieved with the effective suppression of the ridge-splitting phenomenon. Generally speaking, the evolution of the EM field enhancement mode with the dynamic change of the transient permittivity on the material's surface, associated with the pulse-to-pulse surface morphology during the dual-color multipulse pair exposure, is responsible for the control of the ridge-splitting process.

Similarly, both the generation and suppression of the ridge-splitting phenomenon as a function of the pre-irradiated 800 nm laser fluence should also originate from the change of the EM field enhancement mode due to the time-delay-dependent transient permittivity on the material's surface. The density of free electrons excited by the pre-irradiated 800 nm laser is directly proportional to the pulse fluence. The enlargening 800 nm laser fluence causes a decrease of the transient permittivity toward the negative values at the fixed time delay, which supports an opposite evolution tendency for the EM field enhancement mode with the time delay to manipulate the ridge-splitting phenomenon. The increasing fluence of the time-delayed 400 nm laser irradiation is preferable to accelerate the change of the pulse-to-pulse surface morphology, which pushes the evolution of the EM field enhancement mode to strengthen the degree of the ridge-splitting by shortening the time delay during the ablation feedback of the dual-color multipulse pair irradiation.

Our previous investigation has demonstrated that the LIPSSs on the Mo surface induced by a 400 nm wavelength of the femtosecond laser can make the reflectivity decrease by about 25% in the wavelength range of 400−1000 nm,[5] indicating the significant improvement on the solar absorptance. It was recently reported that the LIPSS−Mo surface pair can improve the solar spectral selectivity by a maximum of about 4 times.[28] With the significant performance improvements on solar absorptance and selectivity as well as the high thermal and mechanical stability, the LIPSS−Mo surface pair is the most promising candidate for low-cost, efficient, and high-temperature selective solar absorbers in concentrated solar energy devices. Besides, the LIPSS−Mo surface pair enables other numerous potential applications in antifriction, antibacteria, biocompatibility, superhydrophobicity, etc.

4. CONCLUSIONS

We demonstrated an effective method for the homogeneous nanostructuring of the Mo surface based on the active and dynamic control of the ridge-splitting phenomenon using two-color temporally delayed femtosecond laser pulses of parallel linear polarizations. By properly choosing the time delay and the fluences of the two-color laser pulses, the ridge-splitting phenomenon was manipulated to generate large-area homogeneity. The achieved splitting LIPSS, i.e., the DSL, presents several features, such as a narrow characteristic ridge width of 70 nm, a decreased spatial period of $\Lambda = 140$ nm, and especially the straight and uniform alignment of the grooves associated with the sharp-edge profiles in the long range, which indicates not only the improvement on the structure quality but also the structuring accuracy in the 100 nm scale, in sharp contrast to the result of single-beam femtosecond 400 nm laser pulse irradiation. The uniform distribution of the DSL was identified by the clear discrete frequency spots in the Fourier domain. The experimental results also demonstrated that the generation and suppression of the homogeneous ridge-splitting phenomenon can be manipulated through varying either the time delay or the fluences of the two-color lasers, which results in the transitions between the regular DSL and the NSL. Based on numerical analysis, it was found that the excitation of different types of EM field enhancement modes based on the dynamic change of the transient permittivity and the pulse-to-pulse surface morphology during the transiently correlated dynamic process of the dual laser−material interactions are responsible for the generation and suppression of the homogeneous ridge-splitting phenomenon. The irradiation of dual-color correlated femtosecond laser pulses provides a robust and convenient way for fabricating high-quality 100 nm LIPSSs on metal surfaces, opening up new possibilities in many

https://doi.org/10.1021/acsanm.3c03994
ACS Appl. Nano Mater. 2023, 6, 21092−21100

fields including optoelectronics, tribology, thermology, and biomedicine.

AUTHOR INFORMATION

Corresponding Author

Jianjun Yang − *GPL Photonics Laboratory, State Key Laboratory of Luminescence and Applications, Changchun Institute of Optics, Fine Mechanics and Physics, Chinese Academy of Sciences, Changchun 130033, China; Center of Materials Science and Optoelectronics Engineering, University of Chinese Academy of Sciences, Beijing 100049, China;* orcid.org/0000-0002-6703-4403; Email: jjyang@ciomp.ac.cn

Authors

Bo Zhao − *Laboratory of Optical Field Manipulations, Department of Physics, Changzhi University, Changzhi 046011, China; Advanced Ultraviolet Optoelectronics, Co., Ltd., Changzhi 046000, China;* orcid.org/0000-0002-2020-1809

Ruiping Wang − *Avic Changcheng Institute of Metrology & Measurement, Beijing 100095, China;* orcid.org/0000-0002-8113-3432

Complete contact information is available at: https://pubs.acs.org/10.1021/acsanm.3c03994

Author Contributions

#B.Z. and R.W. contributed equally to this work and should be considered co-first authors.

Notes

The authors declare no competing financial interest.

ACKNOWLEDGMENTS

This work was financially supported by the Applied Basic Research Project of Shanxi Province (No. 20210302124701), the National Key R&D Program of China (No. 2022YFB3604802), the Technology Innovation Center Program of Changzhi (No. 2022cx002), the Strategic Priority Research Program of the Chinese Academy of Sciences (No. XDA220100302), the Scientific and Technological Innovation Programs of the Higher Education Institutions in Shanxi (No. 2022L509), and the Jilin Provincial Science & Technology Development Project (No. 20200201086JC).

REFERENCES

(1) Bonse, J.; Graf, S. Maxwell meets marangoni—a review of theories on laser-induced periodic surface structures. *Laser Photonics Rev.* **2020**, *14*, 2000215.

(2) Stoian, R.; Colombier, J. Advances in ultrafast laser structuring of materials at the nanoscale. *Nanophotonics* **2020**, *9*, 4665−4688.

(3) Zou, T.; Zhao, B.; Xin, W.; Wang, F.; Xie, H.; Li, Y.; Shan, Y.; Li, K.; Sun, Y.; Yang, J. Birefringent response of graphene oxide film structurized via femtosecond laser. *Nano Res.* **2022**, *15*, 4490−4499.

(4) Xie, H.; Zhao, B.; Cheng, J.; Chamoli, S. K.; Zou, T.; Xin, W.; Yang, J. Super-regular femtosecond laser nanolithography based on dual-interface plasmons coupling. *Nanophotonics* **2021**, *10*, 3831−3842.

(5) Zhao, B.; Zheng, X.; Lei, Y.; Xie, H.; Zou, T.; Yuan, G.; Xin, W.; Yang, J. High-efficiency-and-quality nanostructuring of molybdenum surfaces by orthogonally polarized blue femtosecond lasers. *Appl. Surf. Sci.* **2022**, *572*, 151371.

(6) Li, Z.; Wu, Q.; Jiang, X.; Zhou, X.; Liu, Y.; Hu, X.; Zhang, J.; Yao, J.; Xu, J. Formation mechanism of high spatial frequency laser-induced periodic surface structures and experimental support. *Appl. Suf. Sci.* **2022**, *580*, 152107.

(7) Zhao, Z.; Yang, J. Hybrid grating-hole nanostructures produced by spatiotemporal modulation of femtosecond lasers: implications for near-field enhancement. *ACS Appl. Nano Mater.* **2022**, *5*, 9576−9583.

(8) Garcia-Lechuga, M.; Puerto, D.; Fuentes-Edfuf, Y.; Solis, J.; Siegel, J. Ultrafast moving-spot microscopy: birth and growth of laser-induced periodic surface structures. *ACS Photonics* **2016**, *3*, 1961−1967.

(9) Li, Y.; Zhang, X.; Zou, T.; Mu, Q.; Yang, J. Vivid structural color macropatterns created by flexible nanopainting of ultrafast lasers. *ACS Appl. Mater. Interfaces* **2022**, *14*, 21758−21767.

(10) Bonse, J.; Koter, R.; Hartelt, M.; Spaltmann, D.; Pentzien, S.; Hohm, S.; Rosenfeld, A.; Krüger, J. Femtosecond laser-induced periodic surface structures on steel and titanium alloy for tribological applications. *Appl. Phys. A: Mater. Sci. Process.* **2014**, *117*, 103−110.

(11) Liu, N.; Sun, Y.; Wang, H.; Liang, C. Femtosecond laser-induced nanostructures on Fe-30Mn surfaces for biomedical applications. *Opt. Laser Technol.* **2021**, *139*, 106986.

(12) Du, C.; Wang, C.; Zhang, T.; Zheng, L. Antibacterial performance of Zr-BMG, stainless steel, and titanium alloy with laser-induced periodic surface structures. *ACS Appl. Bio Mater.* **2022**, *5* (1), 272−284.

(13) Zorba, V.; Persano, L.; Pisignano, D.; Athanassiou, A.; Stratakis, E.; Cingolani, R.; Tzanetakis, P.; Fotakis, C. Making silicon hydrophobic: wettability control by two-length scale simultaneous patterning with femtosecond laser irradiation. *Nanotechnology* **2006**, *17*, 3234−3238.

(14) Yong, J.; Singh, S. C.; Zhan, Z.; EIKabbash, M.; Chen, F.; Guo, C. Femtosecond-laser-produced underwater "superpolymphobic" nanorippled surfaces: repelling liquid polymers in water for applications of controlling polymer shape and adhesion. *ACS Appl. Nano Mater.* **2019**, *2*, 7362−7371.

(15) Blauner, P. G.; Ro, J. S.; Butt, Y.; Melngailis, J. Focused ion beam fabrication of submicron gold structures. *J. Vac. Sci. Technol. B* **1989**, *7*, 609.

(16) Imboden, M.; Bishop, D. Top-down nanomanufacturing. *Phys. Today* **2014**, *67*, 45−50.

(17) Huang, M.; Cheng, Y.; Zhao, F.; Xu, Z. The significant role of plasmonic effects in femtosecond laser-induced grating fabrication on the nanoscale. *Ann. Phys-Berlin* **2013**, *525*, 74−86.

(18) Yao, J.; Zhang, C.; Liu, H.; Dai, Q.; Wu, L.; Lan, S.; Gopal, A. V.; Trofimov, V. A.; Lysak, T. M. High spatial frequency periodic structures induced on metal surface by femtosecond laser pulses. *Opt. Express* **2012**, *20*, 905−911.

(19) Yu, X.; Zhang, Q.; Qi, D.; Tang, S.; Dai, S.; Zhang, P.; Xu, Y.; Shen, X. Femtosecond laser-induced large area of periodic structures on chalcogenide glass via twice laser direct-writing scanning process. *Opt. Laser Technol.* **2020**, *124*, 105977.

(20) Giannuzzi, G.; Gaudiuso, C.; Franco, C. D.; Scamarcio, G.; Lugara, P. M.; Ancona, A. Large area laser-induced periodic surface structures on steel by bursts of femtosecond pulses with picosecond delays. *Opt. Laser. Eng.* **2019**, *114*, 15−21.

(21) He, W.; Yang, J.; Guo, C. Controlling periodic ripple microstructure formation on 4H-SiC crystal with three time-delayed femtosecond laser beams of different linear polarizations. *Opt. Express* **2017**, *25*, 5156−5168.

(22) Lei, Y.; Yang, J.; Cong, C.; Guo, C. Fabrication of homogenous subwavelength grating structures on metallic glass using double-pulsed femtosecond lasers. *Opt. Laser. Eng.* **2020**, *134*, 106273.

(23) Zhao, B.; Yang, J.; Cheng, J.; Guo, C. Capture of femtosecond plasmon excitation on transient nonequilibrium states of the metal surface. *Phys. Rev. Research* **2020**, *2*, 033418.

(24) Cong, J.; Yang, J.; Zhao, B.; Xu, X. Fabricating subwavelength dot-matrix surface structures of Molybdenum by transient correlated actions of two-color femtosecond laser beams. *Opt. Express* **2015**, *23*, 5357−5367.

(25) Wang, M.; Zhang, N.; Chen, S. C. Effects of supra-wavelength periodic structures on the formation of 1D/2D periodic nanostructures by femtosecond lasers. *Opt. Laser Technol.* **2022**, *151*, 108058.
(26) Zheng, X.; Zhao, B.; Yang, J.; Lei, Y.; Zou, T.; Guo, C. Noncollinear excitation of surface plasmons for triangular structure formation on Cr surfaces by femtosecond lasers. *Appl. Surf. Sci.* **2020**, *507*, 144932.
(27) Giannuzzi, G.; Gaudiuso, C.; Di Mundo, R.; Mirenghi, L.; Fraggelakis, F.; Kling, R.; Lugara, P. M.; Ancona, A. Short and long term surface chemistry and wetting behaviour of stainless steel with 1D and 2D periodic structures induced by bursts of femtosecond laser pulses. *Appl. Surf. Sci.* **2019**, *494*, 1055−1065.
(28) Santagata, A.; Pace, M. L.; Bellucci, A.; Mastellone, M.; Bolli, E.; Valentini, V.; Orlando, S.; Sani, E.; Failla, S.; Sciti, D.; Trucchi, D. M. Enhanced and selective absorption of molybdenum nanostructured surfaces for concentrated solar energy applications. *Materials* **2022**, *15*, 8333.
(29) Sharma, A. K.; Smedley, J.; Tsang, T.; Rao, T. Formation of subwavelength grating on molybdenum mirrors using a femtosecond Ti:sapphire laser system operating at 10 Hz. *Rev. Sci. Instrum.* **2011**, *82*, 033113.
(30) Wang, J.; Guo, C. Numerical study of ultrafast dynamics of femtosecond laser induced periodic surface structure formation on noble metals. *J. Appl. Phys.* **2007**, *102*, 053522.
(31) Gnilitskyi, I.; Derrien, T. J.-Y.; Levy, Y.; Bulgakova, N. M.; Mocek, T.; Orazi, L. High-speed manufacturing of highly regular femtosecond laser-induced periodic surface structures: physical origin of regularity. *Sci. Rep.* **2017**, *7*, 8485.
(32) Huang, M.; Zhao, F.; Cheng, Y.; Xu, N.; Xu, Z. Origin of Laser-induced near subwavelength ripples: interference between surface plasmons and incident laser. *ACS Nano* **2009**, *3*, 4062−4070.
(33) Bonse, J.; Rosenfeld, A.; Krüger, J. On the role of surface plasmon polaritons in theformation of laser-induced periodic surface structures upon irradiation of silicon by femtosecond-laser pulses. *J. Appl. Phys.* **2009**, *106*, 104910.
(34) Fuentes-Edfuf, Y.; Sánchez-Gil, J. A.; Florian, C.; Giannini, V.; Solis, J.; Siegel, J. Surface plasmon polaritons on rough metal surfaces: role in the formation of laser-induced periodic surface structures. *ACS Omega* **2019**, *4*, 6939−6946.
(35) Querry, M. R. *Optical constants of minerals and other materials from the millimeter to the ultraviolet*; CRDEC-CR-88009; Defense Technical Information Center, Chemical Research Development and Engineering Center: Aberdeen, Maryland, 1987.
(36) Cheng, K.; Liu, J.; Cao, K.; Chen, L.; Zhang, Y.; Jiang, Q.; Feng, D.; Zhang, S.; Sun, Z.; Jia, T. Ultrafast dynamics of single-pulse femtosecond laser-induced periodic ripples on the surface of a gold film. *Phys. Rev. B* **2018**, *98*, 184106.
(37) Cheng, K.; Cao, K.; Zhang, Y.; Han, R.; Feng, D.; Liu, J.; Zhang, S.; Sun, Z.; Jia, T. Ultrafast dynamics of subwavelength periodic ripples induced by single femtosecond pulse: from noble to common metals. *J. Phys. D: Appl. Phys.* **2020**, *53*, 285102.
(38) Rudenko, A.; Mauclair, C.; Garrelie, F.; Stoian, R.; Colombier, J.-P. Self-organization of surfaces on the nanoscale by topography-mediated selection of quasi-cylindrical and plasmonic waves. *Nanophotonics* **2019**, *8* (3), 459−465.
(39) Geng, J.; Yan, W.; Shi, L.; Qiu, M. Quasicylindrical waves for ordered nanostructuring. *Nano Lett.* **2022**, *22*, 9658−9663.

https://doi.org/10.1021/acsanm.3c03994
ACS Appl. Nano Mater. 2023, 6, 21092−21100